Interannual Signature in Daily ITCZ States in the East Pacific in Boreal Spring

WENCHANG YANG AND GUDRUN MAGNUSDOTTIR

Department of Earth System Science, University of California, Irvine, Irvine, California

(Manuscript received 18 May 2016, in final form 29 July 2016)

ABSTRACT

The intertropical convergence zone (ITCZ) in the east Pacific is located north of the equator during most of the year. In daily data it is most variable in March–April when it may be located north of the equator (nITCZ), on both sides of the equator (dITCZ), or south of the equator (sITCZ), or it may be absent (when convection does not take on a zonally elongated form). Additionally, in strong El Niño years it is located on the equator during the boreal winter half-year. Here the focus is on conditions when the ITCZ has a presence south of the equator (dITCZ, sITCZ) and composites of various fields are compared to ''normal conditions'' [i.e., when the ITCZ is north of the equator (nITCZ)]. Composites of sea surface temperature (SST), precipitation, outgoing longwave radiation, and the upper-level circulation show very similar patterns for dITCZ and sITCZ days, where the latter cases have almost double the amplitude of the former. The sITCZ state is viewed as an extreme case of the dITCZ state. Both are found to be related to the central Pacific (CP) La Niña with anomalous positive SST and atmospheric heating over the western tropical Pacific and anomalous negative SST and cooling over the central tropical Pacific. Ocean–atmosphere interaction plays an important role in developing the dITCZ and sITCZ anomalies. These daily composite patterns can be reproduced by the regression of monthly fields on the cold CP El Niño–Southern Oscillation mode, suggesting that the interannual rather than day-to-day variability dominates in contributing to the patterns of the composites.

1. Introduction

The tropical Pacific is characterized by different physical processes dominating in the two longitudinal sectors, the west and the east Pacific. Typically, the seasonal cycle in the west is dominated by monsoonal circulations so that during the boreal summer season there is not a well-defined intertropical convergence zone (ITCZ) over the ocean; instead the main convection area is distributed over the continents of southern and eastern Asia. During the boreal summer in the east Pacific, the ITCZ is well defined as a rather narrow, zonally elongated band of convection located to the north of the equator (Bain et al. 2011).

During austral summer, convection is anchored over the Maritime Continent in the west extending eastward at a meridional tilt into the Southern Hemisphere along the South Pacific convergence zone (SPCZ). During the austral summer in the eastern Pacific the ITCZ tends to remain to the north of the equator although with much decreased activity compared to boreal summer. Outside of boreal summer there is considerably more variability in the location of the ITCZ with respect to the equator (Henke et al. 2012; Haffke et al. 2016). On daily time scales the ITCZ may exist in five different states with respect to the equator. The first four are as follws: simultaneously on both sides of the equator (dITCZ), to the north of the equator (nITCZ), to the south of the equator (sITCZ), or the ITCZ may be absent (aITCZ) when the convection is not organized in a longitudinally elongated structure. These were the original four states of the east Pacific ITCZ that were identified by Henke et al. (2012) in five years of daily geostationary satellite data (2000–04). The fifth state was only identified when Haffke et al. (2016) extended the study and analyzed data from 1980 to 2012, years that include strong east Pacific El Niño years such as 1997/98 and 1982/83 and were dominated by a strong east Pacific ITCZ located over the equator (eITCZ, for equatorial ITCZ). The fact that the east Pacific El Niño (EP El Niño; e.g., Kao and Yu 2009) has an ITCZ state all to itself serves as a

Corresponding author address: Wenchang Yang, Department of Earth System Science, University of California, Irvine, 2101E Croul Hall, Irvine, CA 92697.
E-mail: yang.wenchang@uci.edu

DOI: 10.1175/JCLI-D-16-0395.1

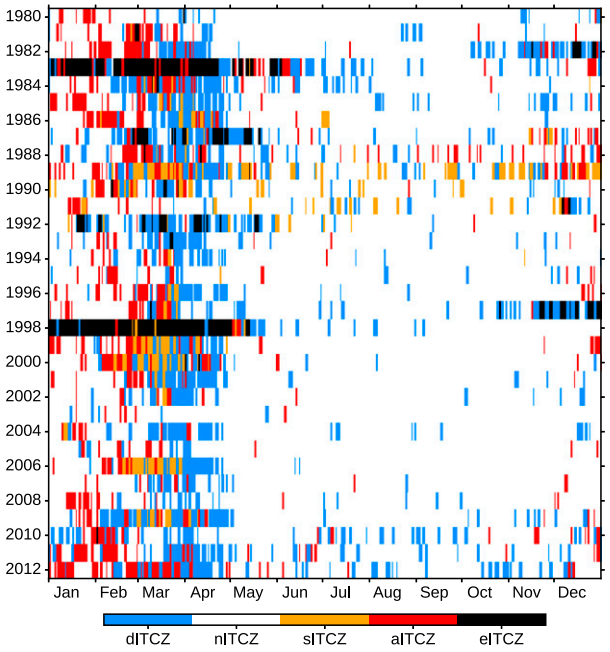

FIG. 1. Daily ITCZ state from 1980–2012 [figure adapted from Fig. 1 in Haffke et al. (2016)]. The vertical axis shows years increasing downward. The horizontal axis shows time of year, labeled by month, increasing toward the right. Each state is represented by a different color: nITCZ = white, dITCZ = blue, sITCZ = yellow, aITCZ = red, and eITCZ = black.

reminder of the dominance of interannual variability associated with El Niño–Southern Oscillation (ENSO) on elongated convection zones over the tropical Pacific. Haffke and Magnusdottir (2013, and references therein) found that the SPCZ tends to stretch from the Maritime Continent in a similarly zonally elongated structure close to the equator during strong El Niños. Therefore, both the east Pacific ITCZ and the SPCZ are associated with equatorial structures during strong EP El Niños. The question is does the central Pacific La Niña (CP La Niña), which is the stronger of the two types of La Niñas (Kao and Yu 2009), also exert an influence on daily states of the east Pacific ITCZ? If there is such an influence, what state of the ITCZ is preferred and how important is this effect? In other words, how can we leverage our understanding of interannual variability of ENSO to better understand the variability of the ITCZ states?

Interest in the variability of the states of the east Pacific ITCZ has mostly focused on a possible fix for the inclination of global climate models to exaggerate the presence of a double ITCZ as it appears in monthly or seasonally averaged data (Zheng et al. 2012; Li and Xie 2014; Li et al. 2015). Such double ITCZ may therefore represent different configurations of all the daily states defined above, as long as the monthly/seasonal mean shows elongated convection on both sides of the equator. In some models this bias is present throughout the annual cycle whereas observations have shown that the dITCZ mostly occurs in March–April or in boreal spring. Figure 1 is reproduced from Haffke et al. (2016) and shows the distribution of daily states of the ITCZ through the annual cycle (January–December, x axis) and from 1980 (top of y axis) to 2012. Certain characteristics are readily apparent. The nITCZ tends to dominate during most of the year, especially outside of boreal late winter to spring. There is a large signature of the prominent EP El Niño events of 1983 and 1998 as the eITCZ dominates in those years, outside of the boreal summer half year. March to April is the time when all states of the ITCZ may occur. Similar to Haffke et al. (2016) we will restrict our study to March–April and we will focus on the two ITCZ states that are present south of the equator, dITCZ and sITCZ. How are those two states of the ITCZ different from the nITCZ that is dominant most of the year? To answer this question we will examine composite anomalies of various fields that are generated by subtracting the fields during nITCZ from the fields during dITCZ and sITCZ. Furthermore, we will examine the contrasts and similarities between the dITCZ and sITCZ anomalies. This paper extends the analysis in Haffke et al. (2016), especially in demonstrating the importance of air–sea interaction on interannual time scales.

The paper is organized as follows. Section 2 describes the data and methods. Section 3 shows results, first as composite anomalies of sea surface temperature (SST), precipitation, outgoing longwave radiation (OLR), and the upper tropospheric circulation. Next, we examine composite anomalies of the surface heat flux as well as the surface wind field. The analysis motivates an examination of the regression of monthly mean fields on the CP La Niña mode in section 4. Section 5 contains concluding remarks.

2. Data and methods

a. Data

The geostationary satellite data used in this study to determine the ITCZ daily states come from the infrared (IR) channel of the GridSat archive (Knapp et al. 2011). This archive goes back to 1980 and represents a collection of satellite images that have been further processed, stitched together, and intercalibrated to form a global dataset that is appropriate for climate studies. The ITCZ states were determined using the statistical model for ITCZ detection described in detail in Haffke et al. (2016) and in Henke et al. (2012). An overview of the distribution of ITCZ states is shown in Fig. 1.

TABLE 1. March–April daily ITCZ state distribution over the years 1980–2012 and 1982–2012.

State	Days 1980–2012	Percentage 1980–2012	Days 1982–2012	Percentage 1982–2012
dITCZ	719	36%	699	37%
nITCZ	755	38%	669	35%
sITCZ	152	8%	152	8%
aITCZ	228	11%	214	11%
eITCZ	159	8%	157	8%

For composite analysis on the dITCZ and sITCZ states and regression analysis the following data are used. Daily SST going back to 1982 is from the NOAA Optimum Interpolation SST (OISST) v2 (Reynolds et al. 2002). Monthly SST is from the NOAA Extended Reconstructed SST (ERSST) v4 (Huang et al. 2015). The field of outgoing longwave radiation (OLR) comes from the NOAA interpolated OLR data (Liebmann and Smith 1996). Even though the original satellite products for this dataset and the GridSat data may have been the same, they were processed differently for the purpose of using for climate studies. For precipitation, atmospheric dynamical fields, and surface heat fluxes, we use the ERA-Interim reanalysis (Dee et al. 2011). The only exception is for the monthly precipitation in the regression analysis, where we use version 2.2 of the Global Precipitation Climatology Project (GPCP) monthly precipitation dataset (Huffman et al. 2009). All datasets are interpolated on a $2° \times 2°$ grid and we focus on the period 1980–2012 except for the OISST data, which are only available from 1982 and we use 1982–2012.

b. *Methods*

For each dataset used in the composite analysis we subtract a 30-day running mean of the daily climatology to eliminate the seasonal cycle. We also eliminate the linear trend at each grid point for each day of these datasets. When examining composite anomalies of daily ITCZ states in Haffke et al. (2016), the reference ITCZ state is an average over all ITCZ states except eITCZ, which is a rarely occurring extreme state. As the most frequently present ITCZ states in March – April are the nITCZ and the dITCZ, the composite anomalies of the different atmospheric and ocean fields show only a small signature due to the dITCZ. Here we take a slightly different approach in the composite analysis. Since we are interested in the dITCZ and sITCZ states (both are present south of the equator) we use the nITCZ as the base from which to calculate anomalies. For the rest of the seasonal cycle, the nITCZ is certainly by far the most dominant state (see Fig. 1). For March–April this method of compositing draws out characteristics of the dITCZ that were not seen in the composite analysis of Haffke et al. (2016).

To examine whether the composites from daily datasets are modulated by the large-scale climate modes of the atmosphere–ocean system on interannual time scales, we compute the first empirical orthogonal function (EOF) of the interannual anomalies of the March–April mean SST over the domain 30°S–30°N, 120°E–80°W, encompassing most of the tropical/subtropical Pacific. Inspired by our SST composite patterns, which are reminiscent of CP La Niña conditions (e.g., Kao and Yu 2009), we regress out the area-averaged SST from the Niño-1+2 region (10°S–0° and 90°–80°W) at each grid point within the EOF domain before conducting the EOF analysis. We use the resulting leading principal component (normalized) to regress various atmospheric and oceanic fields. The regressed fields are compared to the composites from the daily datasets.

3. Composite results

A summary of the distribution of ITCZ states in March–April is shown in Table 1, both for the entire time series of ITCZ states (1980–2012) as well as for the period during which daily SST data are available (1982–2012). The nITCZ and dITCZ dominate variability in spring, at 38% (35%) and 36% (37%), respectively for the two periods. As stated above, to draw out variability associated with the dITCZ state, we use the nITCZ state as the background that we subtract to obtain anomalies in the composite analysis. The fact that the nITCZ state dominates during other parts of the year is further justification for using it as the ''normal'' state. In this study our focus is on the ITCZ states that have presence south of the equator, the dITCZ and the sITCZ.

Figure 2 shows histograms of daily precipitation difference between the southern region (14°S–0°) and the northern region (0°–14°N) over the east Pacific (150°–90°W) for composites belonging to the three ITCZ states, nITCZ, dITCZ, and sITCZ. The small panel in Fig. 2 shows the location of the two sectors in the east Pacific. Note that according to Table 1, the fraction of days belonging to sITCZ (8%) is much less than the fraction of days belonging to nITCZ (38%) and dITCZ (36%). The total contribution to precipitation is therefore much less for sITCZ (area under red curve in Fig. 2). The main point of Fig. 2 is to show the asymmetry in the precipitation with respect to the equator for the three states. Note that 84% of the days with nITCZ have a negative precipitation asymmetry and the mean value is $-1.4\,\mathrm{mm\,day^{-1}}$. This is expected for the nITCZ when the elongated band of convection is located north of the equator. In the case of the sITCZ, the mean value

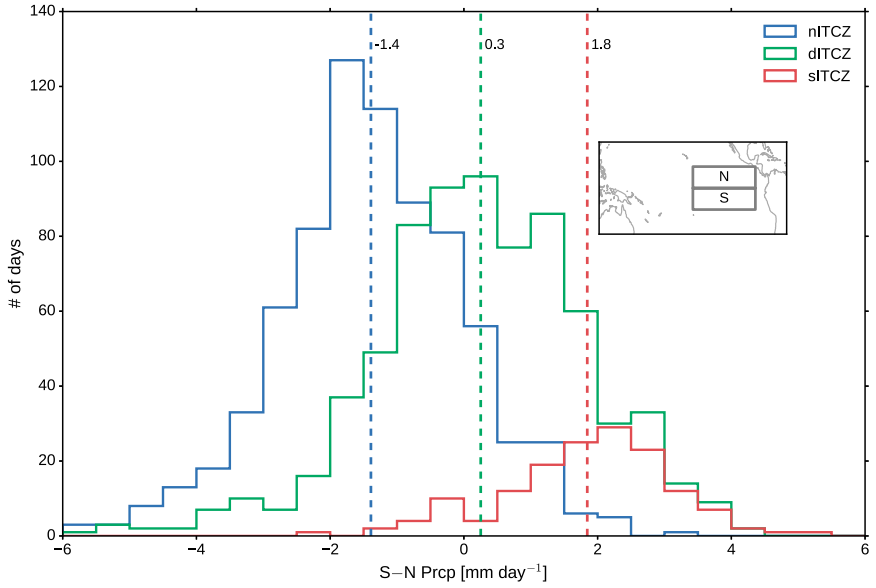

FIG. 2. Histograms of daily precipitation difference: the strip north of the equator (region N; 0°–14°N) subtracted from the strip south of the equator (region S; 14°S–0°) over the east Pacific (150°–90°W). The boundaries for the two regions N and S are shown in the smaller panel.

shifts to the positive side or 1.8 mm day^{-1} and only 11% of the days have more precipitation to the north of the equator than to the south. Interestingly, the distribution is asymmetric for dITCZ such that there is a preference for more precipitation to be located in the Southern Hemisphere, with a mean value of 0.3 mm day^{-1} and only 43% of the days have more precipitation to the north of equator. According to equatorial asymmetry in precipitation, dITCZ is more like sITCZ than nITCZ. This will be expanded on when we examine spatial distribution of composite anomalies due to dITCZ and sITCZ in the different atmospheric and oceanic fields.

a. Composites of SST, precipitation, atmospheric heating, and circulation

Figure 3a shows the composite anomaly over dITCZ days (compared to nITCZ days) for SST.

Over the east Pacific (east of 120°W), SST is anomalously cool to the north and warm over the area south of the equator, which is consistent with the enhanced convection to the south of the equator for the dITCZ state. Another prominent feature of the SST composite is the cooling over the tropical central Pacific centered around the date line, in contrast to the warming over the tropical western Pacific that extends eastward and poleward into the subtropics. This distinctive SST composite pattern for the dITCZ resembles the CP La Niña as shown in Fig. 10d of Kao and Yu (2009). This suggests that the dITCZ state may be associated with CP La Niña conditions. Moving to the sITCZ as shown in Fig. 3b, the SST composite pattern is strikingly similar to that for the dITCZ: warm south and cool north of the equator in the east Pacific, and a warm western Pacific in contrast to cool central Pacific. The difference is in the magnitude: for the sITCZ composite anomalies, SST anomalies are nearly twice as strong as those associated with the dITCZ composite anomalies. The striking resemblance between the dITCZ and sITCZ in the SST composites and the much larger magnitude in the sITCZ suggest that the sITCZ may be an extreme case of the dITCZ.

Figures 3c and 3d show composite anomalies in precipitation, an important proxy for atmospheric convection and heating, for the dITCZ and sITCZ, respectively. Upon examining the figures the first impression is that the sITCZ pattern is very similar to the dITCZ while the magnitude is again about twice as large, consistent with the SST composites. Also consistent with the SST composites are the enhanced precipitation to the south of the equator and suppressed precipitation north of the equator over the tropical east Pacific. Furthermore, the precipitation anomalies are positive over the western tropical Pacific but negative over the central tropical Pacific, consistent with the CP La Niña SST configuration. The major difference between the precipitation and SST composites is that the former shows large and significant values mostly within the tropics, whereas the latter has a more global distribution. This is because the tropical precipitation is in general predominant compared to precipitation at higher latitudes.

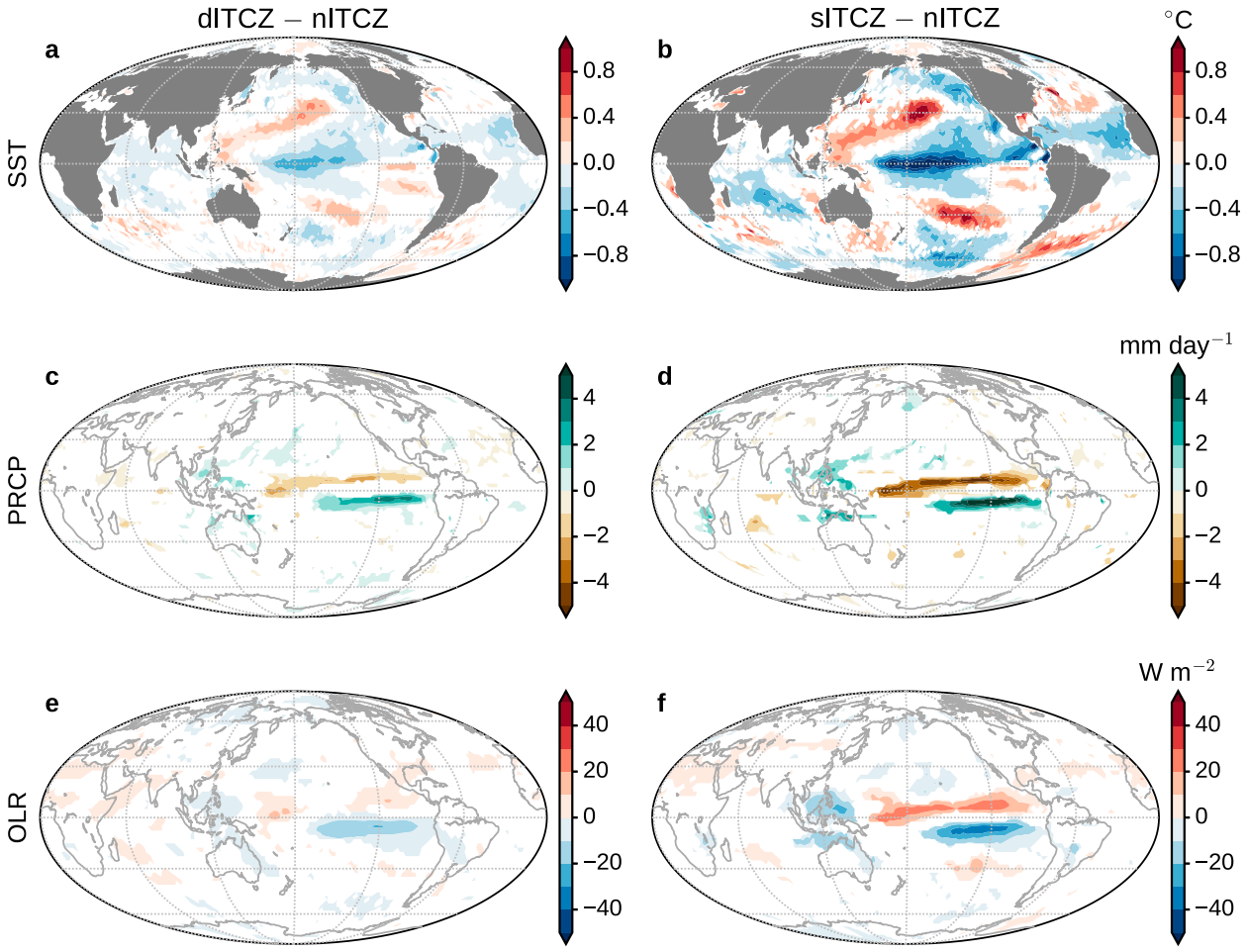

FIG. 3. Composites of March–April daily fields for days categorized as (left) dITCZ and (right) sITCZ, both relative to the March–April mean for nITCZ. The fields are (a),(b) SST, (c),(d) precipitation, and (e),(f) OLR. All fields are for 1980–2012 except SST in (a) and (b) is for 1982–2012. Shaded areas are significant at the 0.05 level by a two-sided Student's *t* test.

The OLR is composited for anomalies in dITCZ and sITCZ and shown in Figs. 3e and 3f, respectively, where negative values indicate anomalous high cloudiness and enhanced convection centers and positive values the lack thereof or atmospheric cooling. To the first order, the OLR composites mirror the precipitation patterns described above, with atmospheric heating over the west Pacific and to the south of the equator over the east Pacific, but cooling over the central tropical Pacific as well as to the north of the equator over the east Pacific. Again, the magnitude of heating and cooling for the sITCZ is larger than that for the dITCZ. The OLR composites differ from those of precipitation only in the smoothness of the field. While the precipitation anomaly centers are sharp and concentrated near the equator, the OLR composites are much smoother and spread into the subtropics.

The superimposed anomalous heating will inevitably drive an anomalous atmospheric circulation as illustrated by simple models of the tropical atmosphere (e.g., Gill 1980). Figure 4a shows the dITCZ and nITCZ composites of 200-hPa atmospheric circulation as represented by streamfunction (shading) and horizontal wind (vectors). The influence from the heating and cooling sources is readily apparent. The heating over the western Pacific induces easterlies over the tropical eastern Indian Ocean as well as two anticyclonic centers, one in each hemisphere. The Northern Hemisphere one is to the northwest of the heating source centered at the southeastern coast of China and the second is to the southwest of the heating source off the west coast of Australia. The west Pacific heating together with the cooling around the equator close to the date line also induce a long track of westerlies along the equator over the central and east Pacific, especially to the north of the equator.

The westerlies are not apparent to the south of the equator because of the existence of new heating and cooling sources over the east Pacific. The equatorially

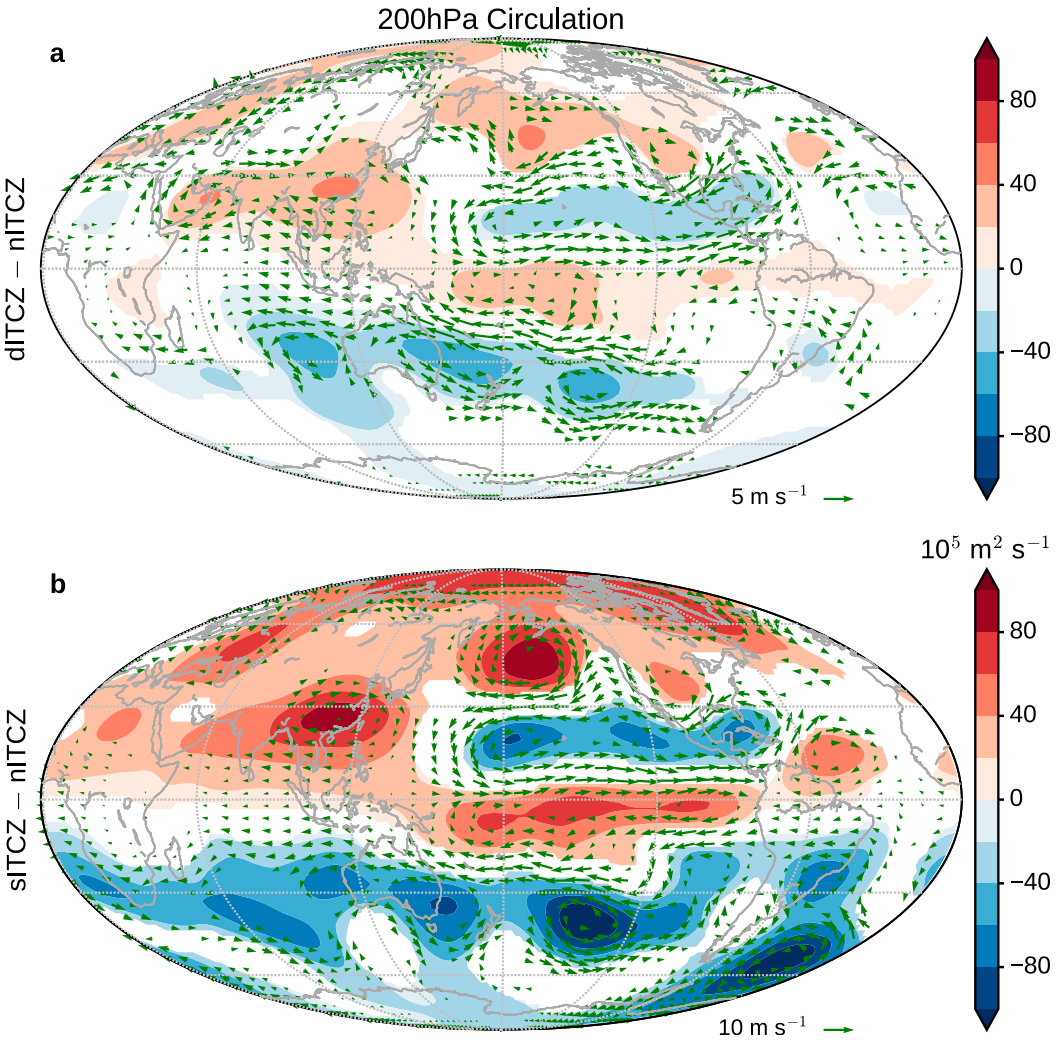

FIG. 4. As in Fig. 3, but for the fields of 200-hPa streamfunction (shaded) and wind velocity (vectors), with composites shown for (a) dITCZ and (b) sITCZ days.

asymmetric heating/cooling patterns over the east Pacific lead to anomalous easterlies between the equator and the Southern Hemisphere heating center and westerlies to the north of the equator. This strengthens the north-of-equator westerlies over the central and east Pacific, but weakens the south-of-equator westerlies or even reverses them to easterlies. As a result, the tropical westerlies over the central and east Pacific move off the equator and northward. All the features described above can also be found in the sITCZ–nITCZ composite in Fig. 4b, except at almost double the amplitude. This is consistent with the heating contrast (or OLR) between the sITCZ and dITCZ composite anomalies in Figs. 3e and 3f.

Two points can be made from composites in Figs. 3 and 4. First, composites for the sITCZ state closely resemble the patterns for the dITCZ state. In fact, the spatial pattern correlations between dITCZ and sITCZ composites for SST, precipitation, OLR, and 200-hPa streamfunction are 0.81, 0.68, 0.76, and 0.82, respectively. The composites for the two states differ in magnitude such that sITCZ anomaly fields are considerably stronger than dITCZ anomaly fields. In other words, the sITCZ can be treated as the extreme case of the dITCZ. From here on we shall focus on the extreme case sITCZ–nITCZ for composite analysis. The second point is that the dITCZ and sITCZ states are closely related to the CP La Niña–like SST configuration and the associated atmospheric heating and circulation. For example, the enhanced convection to the south of the equator, over the east Pacific appears to be linked to the increased heating over the west Pacific and suppressed heating over the tropical central Pacific. Lietzke et al. (2001) point to the importance of the state of ENSO in

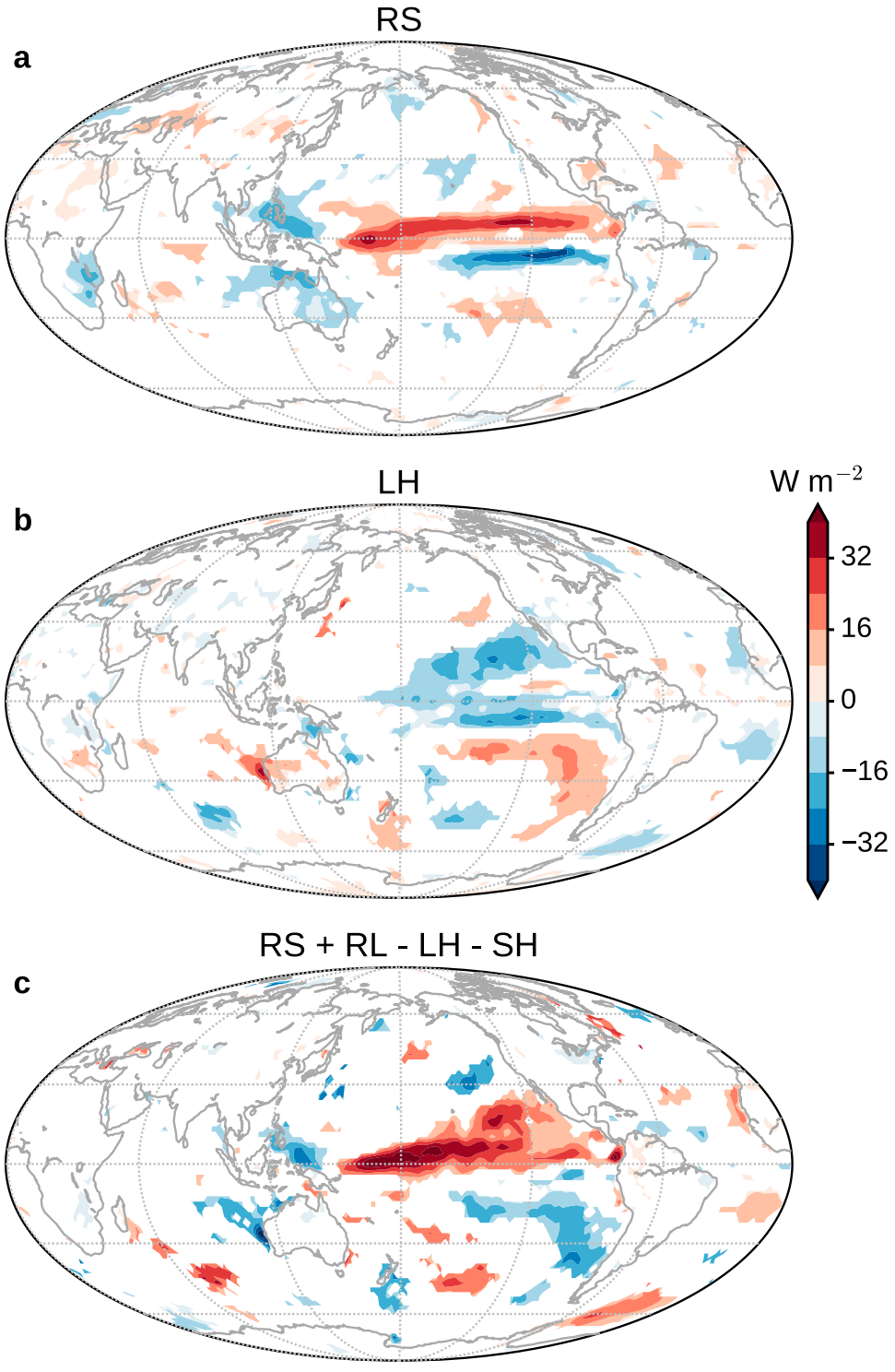

FIG. 5. Composites of March–April daily fields for days categorized as the sITCZ. (a) Net surface shortwave radiative flux (RS), (b) latent heat flux (LH), and (c) total heat flux (RS + RL − LH − SH, where RL is the net longwave radiative flux and SH is the sensible heat flux). The net radiative fluxes are defined positive downward, while the latent and sensible heat fluxes are defined positive upward. Shaded areas also indicate that they are statistically significant at the 0.05 level by a two-sided Student's *t* test.

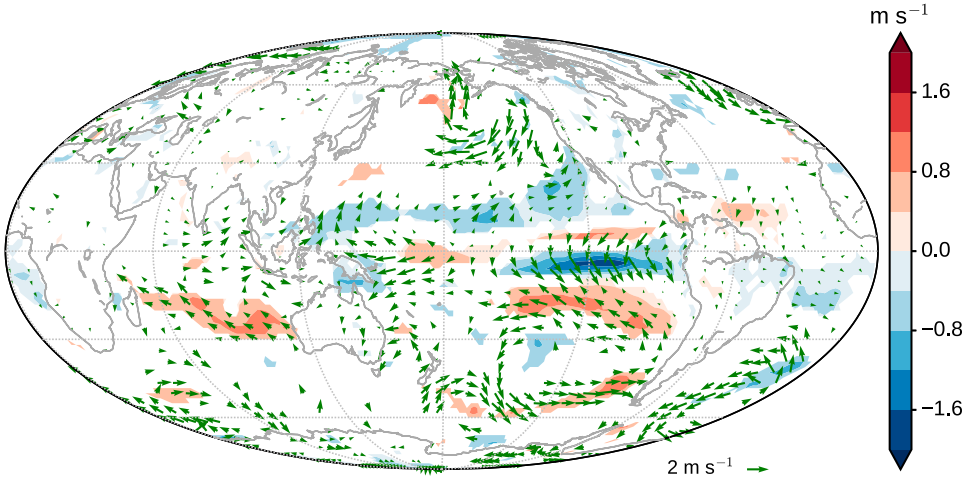

FIG. 6. As in Fig. 5, but for 10-m wind speed (shaded) and velocity (vectors).

terms of development of a spring double ITCZ, stating that it is more likely to occur in La Niña years when the equatorial cold tongue in the east Pacific is strong.

b. *Composites of surface heat fluxes*

Figure 5 shows composites of components of the surface heat flux for sITCZ–nITCZ. The dITCZ composites (not shown) are very similar to the sITCZ results but with a weaker magnitude. The radiation fluxes are defined positive downward while for the latent and sensible heat fluxes we follow convention and define them positive upward. Figures 5a and 5b show the net shortwave radiation (RS) and latent heat flux (LH), respectively. The surface heat flux over the ocean is dominated by the net shortwave radiative flux and the latent heat flux, with the net longwave radiative flux and sensible heat flux secondary and not shown here. The net shortwave radiation composite (Fig. 5a) is consistent with the shift in convection and precipitation for the sITCZ as shown in Figs. 3d and 3f, or reduced over the convection enhanced regions (the western Pacific and to the south of the equator over the east Pacific) and strengthened over the convection suppressed regions (the central tropical Pacific and to the north of the equator over the east Pacific). The latent heat flux (Fig. 5b) shows a different spatial pattern from the net shortwave radiation. It is enhanced to the south of 15°S over the east Pacific and extends to latitudes as high as 60°S over the southeast Pacific. To the north of 15°S within the tropics, the latent flux is in general suppressed except for a narrow band near 10°N.

Figure 5c shows the sum of the four components of the surface heat flux, where the sign convention is positive downward. A prominent downward total heat flux anomaly emerges over the equatorial central Pacific centered around the date line, which has opposite sign to that of the SST composite in the same region in Fig. 3b. The eastern and western Pacific regions also have opposite signs when compared to the SST composite in the same region, suggesting that the SST anomalies in Fig. 3b are driven not by surface heat fluxes but by ocean dynamical processes, which in turn may be driven by surface winds (Fig. 6). Over the equatorial central Pacific, centered around the date line, the surface winds are divergent and could induce upwelling and develop cooling of SST. Over the tropical east Pacific, divergent northeasterly anomalies develop to the north of the equator, turn to northwesterlies after crossing the equator, and converge with the southeasterlies at around 10°S. The divergent surface winds to the north of the equator and the convergent surface winds to the south could also induce local upwelling to the north and downwelling to the south leading to the SST anomalies in Fig. 3b.

A positive feedback mechanism that has great impact in the tropics is the wind–evaporation–SST (WES) feedback (e.g., Xie and Philander 1994). It states that higher SST on one side of the equator favors an ITCZ located on that side of the equator and this will in turn reinforce its location due to increased wind speed and hence increased latent heat flux and SST cooling in the areas that feed into the ITCZ. The WES mechanism also seems to work here since the wind speed increases to the north of the equator and decreases to the south, consistent with the SST cooling to the north and warming to the south as shown in Figs. 3b. Farther from the equator, Ekman flow induced by the surface winds may also contribute to the SST anomalies by advection. Note that the wind speed of the southeasterlies to the south of 10°S also intensifies, consistent with the latent heat flux

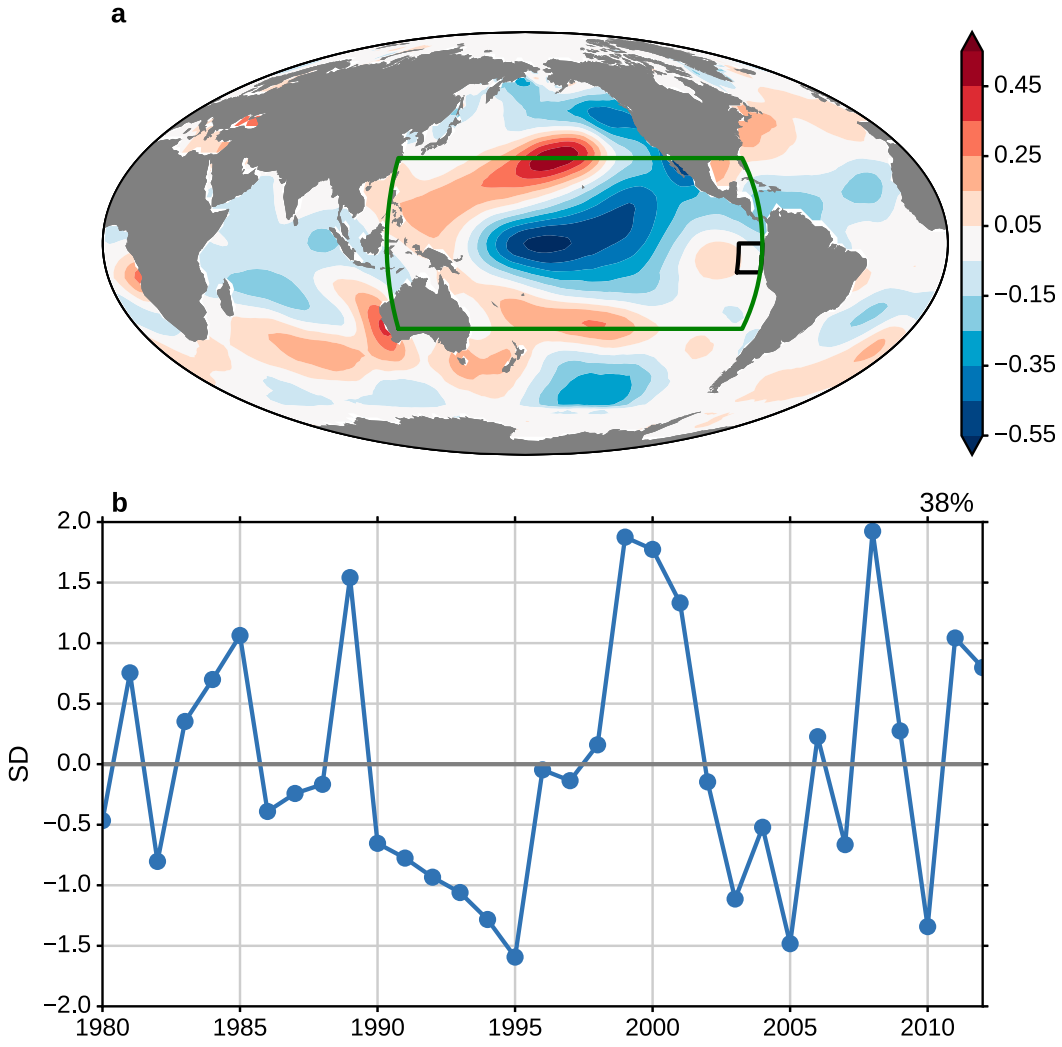

FIG. 7. EOF analysis of the March–April seasonal mean tropical Pacific SSTs over 30°S–30°N, 120°E–80°W (the green box in the upper panel) after the area-averaged SSTs over the Niño-1+2 region (10°S–0°, 90°–80°W, the black box in the upper panel) has been regressed out at each grid point. (a) Regression of global March–April seasonal mean SSTs on the normalized leading principal component. (b) The normalized leading principal component.

composite in Fig. 5b. These latent heat flux enhanced regions serve as the moisture source for the enhanced convection and precipitation center to the south of the equator.

4. The central Pacific La Niña mode

Composite anomalies associated with the two daily ITCZ states, dITCZ and sITCZ (in SST, precipitation, and OLR) are similar in pattern but the anomalies due to dITCZ are about half the amplitude of the anomalies due to sITCZ. Both are reminiscent of those due to the CP La Niña coupled climate mode as we discussed in section 3a. Here we want to attempt to quantify the degree to which the sITCZ state in March to April may be associated with CP La Niña. The approach is as follows: We compute the EOF of SST inside the region demarcated in green in Fig. 7a, after subtracting the regression of the area-mean SST in the Nino-1+2 region (shown by black outline in the far eastern Pacific in the same figure) with SST in the rest of the green outlined region. In other words, we perform the EOF analysis on SST of the residual field, thereby removing the influence of the Niño-1+2 region (or EP ENSO). The resulting normalized principal component of the leading mode is shown in Fig. 7b. It explains 38% of the total variance. Figure 7a shows the regression of global SST on the normalized leading principal component and it largely resembles the SST composites for the dITCZ (Fig. 3a) and sITCZ (Fig. 3b). Even outside of the Pacific, the

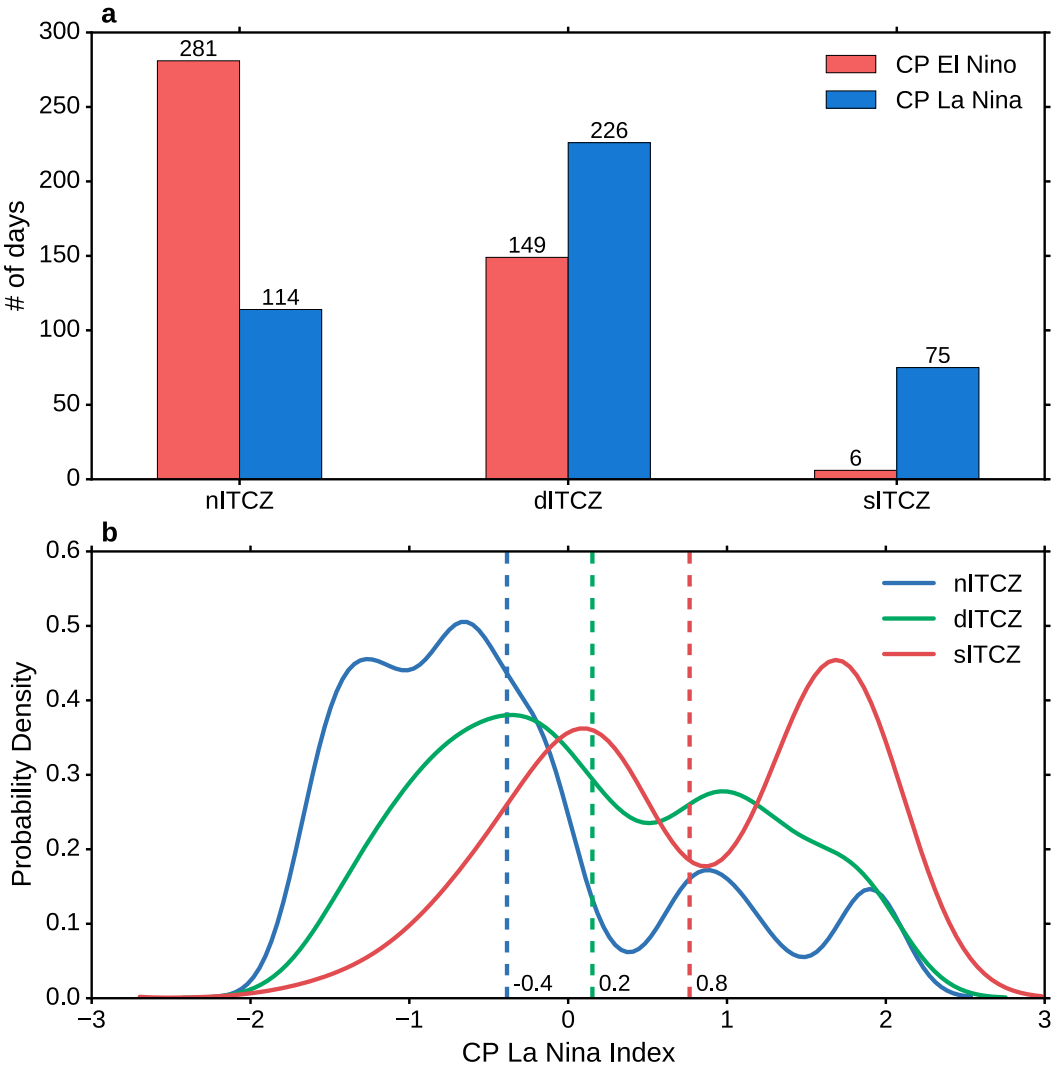

FIG. 8. Relationship between the CP La Niña index and the ITCZ (daily) state. (a) Number of days of nITCZ, dITCZ, and sITCZ for CP El Niño (red) vs CP La Niña (blue) years. The CP La Niña (El Niño) years are defined as the years when the leading principal component in Fig. 7b is greater than its upper (less than its lower) quartile. This definition yields 8 years of CP La Niña (1985, 1989, 1999, 2000, 2001, 2008, 2011, 2012) and 8 years of CP El Niño (1982, 1992, 1993, 1994, 1995, 2003, 2005, 2010). (b) Probability density of the CP La Niña index for nITCZ, dITCZ, and dITCZ. The probability is estimated based on the kernel density estimation. The CP La Niña index is defined as the normalized leading principal component in Fig. 7b. Vertical dashed lines show the mean values for each distribution.

regressed SSTs are generally in line with the SST composites for the dITCZ and sITCZ. It suggests that the composites for the dITCZ and sITCZ may be due to similar mechanisms as the CP La Niña.

In an attempt to quantify the relationship between the CP La Niña and nITCZ/dITCZ/sITCZ states we chose years when the principal component is less than its lower quartile (CP El Niño) and greater than its upper quartile (CP La Niña). This results in eight years of CP El Niño (1982, 1992, 1993, 1994, 1995, 2003, 2005, and 2010) and eight years of CP La Niña (1985, 1989, 1999, 2000, 2001, 2008, 2011, and 2012). Figure 8a shows the ITCZ daily state distribution (for nITCZ, dITCZ, and sITCZ) for CP El Niño and CP La Niña. The nITCZ days decrease by 60% from CP El Niño to CP La Niña years, whereas the dITCZ days increase by more than 50%. Most strikingly, the sITCZ days jump by an order of magnitude, from 6 to 75, suggesting that the sensitivity of sITCZ state to the CP La Niña conditions is much greater than that of the dITCZ.

Another way of illustrating the relationship between CP La Niña conditions and the ITCZ daily states is to

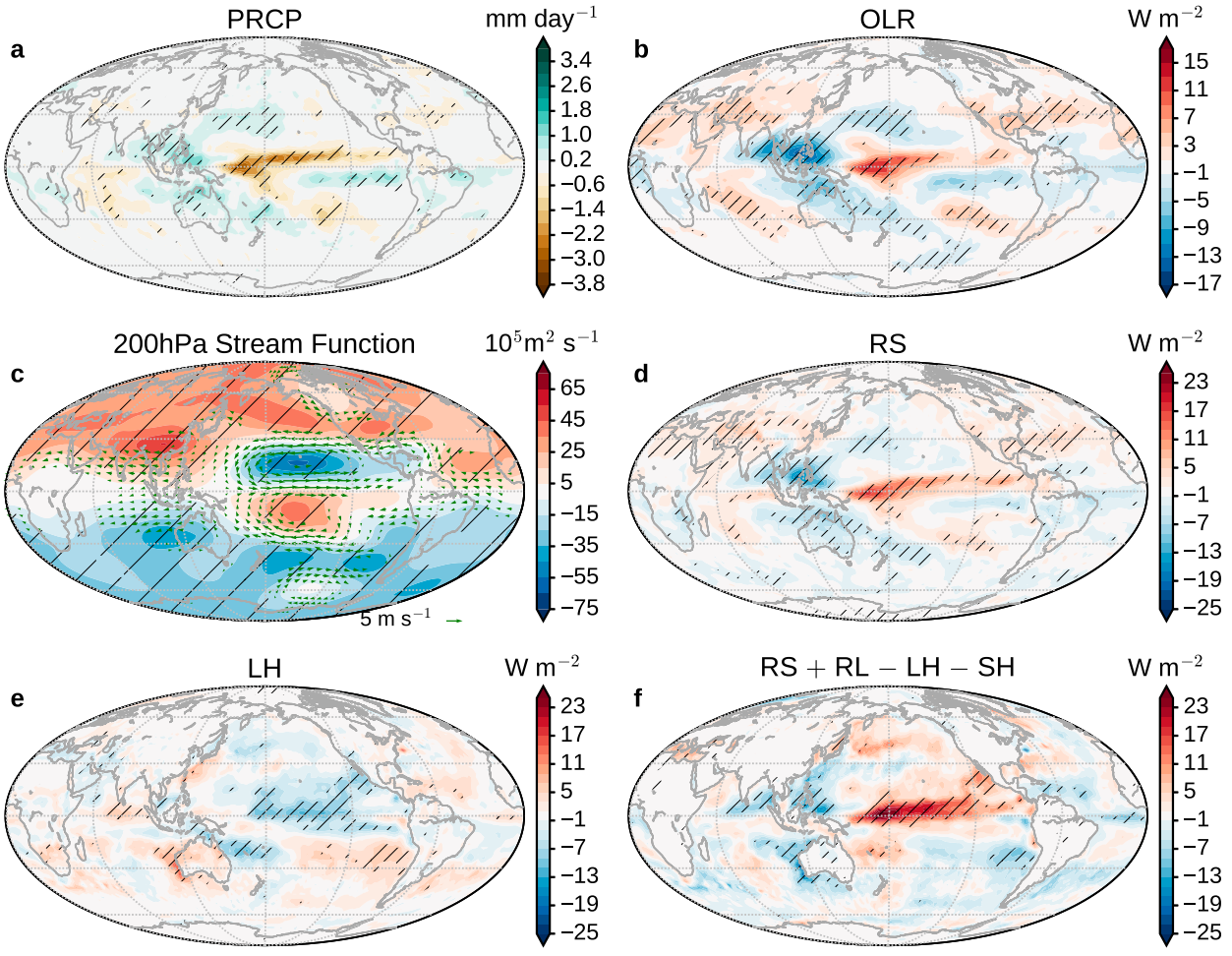

FIG. 9. Regression of various March–April seasonal mean observed fields on the normalized leading principal component in Fig. 7b: (a) GPCP precipitation, (b) outgoing longwave radiation (OLR); (c) 200-hPa streamfunction (shaded) and wind velocity (vectors), (d) net surface shortwave radiative flux (RS, positive downward), (e) latent heat flux (LH, positive upward), and (f) total surface heat flux (RS + RL − LH − SH, positive downward). Hatching indicates where the value is significant at the 0.05 level by a two-sided Student's *t* test.

look at the distribution of the CP La Niña index for days of each daily ITCZ state as shown in Fig. 8b. The CP La Niña index is defined directly from the normalized leading principal component in Fig. 7b. From Fig. 8b, we can see that starting from nITCZ to dITCZ and then to sITCZ, the probability density curve moves gradually to the positive (right) side. The mean CP La Niña index for nITCZ is −0.4, for dITCZ it is 0.2, and for sITCZ it is 0.8. In other words, days of sITCZ are likely to have a higher CP La Niña index than days of nITCZ. Both Figs. 8a and 8b suggest that daily ITCZ states are modulated by the large-scale CP ENSO mode. More specifically, the CP La Niña condition favors the dITCZ and sITCZ daily states.

Regression of atmospheric fields on the CP La Niña mode

To further convince readers of the connection between CP La Niña and the sITCZ state we now show regression analysis on the normalized leading principal component. Figure 9 shows the regression of some of the same fields as were previously depicted through composite analysis, where statistically significant areas, at the 0.05 level by the two-sided Student's *t* test, are hatched. The regressed precipitation (Fig. 9a) is to a large extent similar to the daily composites in Figs. 3c and 3d. It is enhanced to the south of the equator over the east Pacific and suppressed to the north of the equator. The regressed precipitation is also suppressed over the central tropical Pacific around the date line but enhanced over the western Pacific and the Maritime Continent. All these features are present in the dITCZ/sITCZ composite maps from daily data. Similarly, the regressed OLR field (Fig. 9b) also indicates the same enhanced and suppressed convection centers as the daily composites in Figs. 3e and 3f. The main difference is that the regressed heating center over the western Pacific and the Maritime Continent is much stronger than

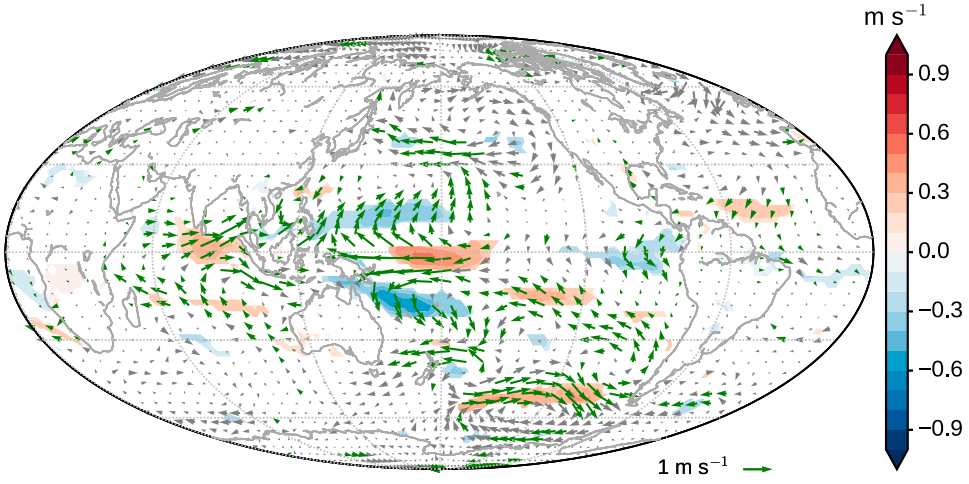

FIG. 10. As in Fig. 9, but for 10-m wind speed (shaded) and velocity (vectors). Green vectors indicate that at least one of its two components is significant at the 0.05 level by a two-sided Student's *t* test.

that to the south of the equator in the east Pacific, whereas for the daily composites the two heating centers are comparable. The regressed 200-hPa circulation is also similar to the composite results in Fig. 4.

The regressed surface heat fluxes are dominated by the net shortwave radiation (Fig. 9d) and the latent heat flux (Fig. 9e), similar to the composited fields in Figs. 5a and 5b. The net longwave radiation and sensible heat flux are secondary (not shown here). The regressed net shortwave radiation is similar to the daily composite in Fig. 5a except the reduced downward radiation to the south of the equator over the east Pacific is weak compared to the western Pacific. Similarly the regressed latent heat flux in Fig. 9e parallels the composited one in Fig. 5b except for the weaker signal in the east Pacific. The total surface heat flux shown in Fig. 9f also captures the major features in the composite result in Fig. 5c.

Finally, the major features found in the daily composites of the 10-m winds in Fig. 6 can also be seen in the regressed 10-m wind field in Fig. 10, including the divergent winds over the central tropical Pacific around the date line and the northerly winds crossing the equator that converge with the southeasterlies at around 10°S over the east Pacific. All these similarities between the regressed fields and the corresponding daily composites suggest that the distinctive daily composites for the dITCZ and sITCZ may be associated with the CP La Niña condition as revealed from the monthly dataset. In other words, interannual variability of the CP La Niña contributes dominantly to the patterns of the composites for the daily dITCZ and sITCZ.

5. Concluding remarks

Henke et al. (2012) introduced a sophisticated statistical model to automatically detect the features of the ITCZ over the east Pacific from 3-hourly satellite images and categorize the ITCZ at each time point. Extending and applying this method on satellite images over the period of 1980–2012, Haffke et al. (2016) summarized the statistics of the identified instantaneous ITCZs and performed some preliminary composite analysis for different states of the east Pacific ITCZ during March and April. In this study, we extend the work of Haffke et al. (2016) by concentrating on the states of the ITCZ that have a component south of the equator and determining how during March–April they are different from the nITCZ state, which is by far the most prevalent ITCZ state at other times of the year, outside of EP El Nina years when the eITCZ dominates outside of summer. We examine composites of various atmospheric and oceanic fields for the dITCZ and sITCZ deviated from the nITCZ to highlight differences from the "normal" state. In particular, we emphasize composites of components of the surface heat flux as well as examining the correspondence between the composites and the interannual variability of the large-scale climate mode due to CP La Niña. Our findings are as follows:

- The dITCZ and sITCZ states are related to CP La Niña conditions, with anomalous positive SSTs and atmospheric heating over the western tropical Pacific and anomalous negative SSTs and atmospheric cooling over the central tropical Pacific.
- The composites for the sITCZ are similar in pattern with those for the dITCZ but greater in magnitude. The sITCZ is the extreme case of the dITCZ.
- Ocean–atmosphere interaction plays an important role in developing the dITCZ and sITCZ anomalies.
- The patterns of the daily composites can largely be reproduced by the monthly datasets, through the

regression of these datasets on the central Pacific La Niña mode.

The ITCZ over the east Pacific is a complex phenomenon that is highly interactive with other components of the climate system. In this study, we find that during boreal spring, the daily ITCZ states of dITCZ and sITCZ are closely related to CP La Niña condition. This is consistent with an earlier observational study (Lietzke et al. 2001), where the double ITCZ was shown to be favored during La Niña years when the Pacific cold tongue is strong. Interestingly, some global climate models are disposed to two biases simultaneously, an excessive cold tongue and too prevalent a convection zone south of the equator in the tropical east Pacific (Zheng et al. 2012; Li and Xie 2014; Li et al. 2015). The coexistence of the cold tongue and the double ITCZ in both observations and models suggests that they may be driven by similar physical mechanisms. It is also quite plausible that there is a stochastic element to the distribution of daily ITCZ states. However, this does not mean that the prevalence of the dITCZ and sITCZ states may lead to a CP La Niña.

Acknowledgments. This research was supported by NSF Grants AGS-1206120 and AGS-1407360. We thank Colene Haffke and Daniel Henke as well as two anonymous reviewers for helpful comments on the manuscript.

REFERENCES

Bain, C., J. De Paz, J. Kramer, G. Magnusdottir, P. Smyth, H. Stern, and C.-C. Wang, 2011: Detecting the ITCZ in instantaneous satellite data using spatiotemporal statistical modeling: ITCZ climatology in the east Pacific. *J. Climate*, **24**, 216–230, doi:10.1175/2010JCLI3716.1.

Dee, D. P., and Coauthors, 2011: The ERA-Interim reanalysis: Configuration and performance of the data assimilation system. *Quart. J. Roy. Meteor. Soc.*, **137**, 553–597, doi:10.1002/qj.828.

Gill, A. E., 1980: Some simple solutions for heat-induced tropical circulation. *Quart. J. Roy. Meteor. Soc.*, **106**, 447–462, doi:10.1002/qj.49710644905.

Haffke, C., and G. Magnusdottir, 2013: The South Pacific convergence zone in three decades of satellite images. *J. Geophys. Res. Atmos.*, **118**, 10 839–10 849, doi:10.1002/jgrd.50838.

——, ——, D. Henke, P. Smyth, and Y. Peings, 2016: Daily states of the March–April east Pacific ITCZ in three decades of high-resolution satellite data. *J. Climate*, **29**, 2981–2995, doi:10.1175/JCLI-D-15-0224.1.

Henke, D., P. Smyth, C. Haffke, and G. Magnusdottir, 2012: Automated analysis of the temporal behavior of the double Intertropical Convergence Zone over the east Pacific. *Remote Sens. Environ.*, **123**, 418–433, doi:10.1016/j.rse.2012.03.022.

Huang, B., and Coauthors, 2015: Extended reconstructed sea surface temperature version 4 (ERSST.v4). Part I: Upgrades and intercomparisons. *J. Climate*, **28**, 911–930, doi:10.1175/JCLI-D-14-00006.1.

Huffman, G. J., R. F. Adler, D. T. Bolvin, and G. Gu, 2009: Improving the global precipitation record: GPCP version 2.1. *Geophys. Res. Lett.*, **36**, L17808, doi:10.1029/2009GL040000.

Kao, H.-Y., and J.-Y. Yu, 2009: Contrasting eastern-Pacific and central-Pacific types of ENSO. *J. Climate*, **22**, 615–632, doi:10.1175/2008JCLI2309.1.

Knapp, K. R., and Coauthors, 2011: Globally gridded satellite observations for climate studies. *Bull. Amer. Meteor. Soc.*, **92**, 893–907, doi:10.1175/2011BAMS3039.1.

Li, G., and S.-P. Xie, 2014: Tropical biases in CMIP5 multimodel ensemble: The excessive equatorial Pacific cold tongue and double ITCZ problems. *J. Climate*, **27**, 1765–1780, doi:10.1175/JCLI-D-13-00337.1.

——, Y. Du, H. Xu, and B. Ren, 2015: An intermodel approach to identify the source of excessive equatorial Pacific cold tongue in CMIP5 models and uncertainty in observational datasets. *J. Climate*, **28**, 7630–7640, doi:10.1175/JCLI-D-15-0168.1.

Liebmann, B., and C. Smith, 1996: Description of a complete (interpolated) outgoing longwave radiation dataset. *Bull. Amer. Meteor. Soc.*, **77**, 1275–1277.

Lietzke, C. E., C. Deser, and T. H. Vonder Haar, 2001: Evolutionary structure of the eastern Pacific double ITCZ based on satellite moisture profile retrievals. *J. Climate*, **14**, 743–751, doi:10.1175/1520-0442(2001)014<0743:ESOTEP>2.0.CO;2.

Reynolds, R. W., N. A. Rayner, T. M. Smith, D. C. Stokes, and W. Wang, 2002: An improved in situ and satellite SST analysis for climate. *J. Climate*, **15**, 1609–1625, doi:10.1175/1520-0442(2002)015<1609:AIISAS>2.0.CO;2.

Xie, S.-P., and S. G. H. Philander, 1994: A coupled ocean–atmosphere model of relevance to the ITCZ in the eastern Pacific. *Tellus*, **46A**, 340–350, doi:10.1034/j.1600-0870.1994.t01-1-00001.x.

Zheng, Y., J.-L. Lin, and T. Shinoda, 2012: The equatorial Pacific cold tongue simulated by IPCC AR4 coupled GCMs: Upper ocean heat budget and feedback analysis. *J. Geophys. Res.*, **117**, C05024, doi:10.1029/2011JC007746.